JOURNAL OF THERMOPHYSICS AND HEAT TRANSFER
Vol. 15, No. 1, January–March 2001

Computation of Hypersonic Radiating Flowfield over a Blunt Body

Takeharu Sakai,* Tomoko Tsuru,† and Keisuke Sawada‡
Tohoku University, Sendai 980-8579, Japan

A numerical method for calculating a strongly radiating axisymmetric flowfield is developed. Radiative transfer is treated one, two, and three dimensionally. Radiative heat flux is evaluated using a model developed earlier that combines Planck, Rosseland, and gray-gas models. The flow solution is obtained with a fully implicit time-marching method using a full block matrix inversion. To show its robustness the method is applied to calculate the environment of a blunt body flying at the velocity of 16 km/s. The results show that the multidimensional radiative transport calculation is different from the one-dimensional calculation. The computational costs for the method are given for each method of radiative transfer calculations. The method is also tested for an experiment conducted in a ballistic range. The calculated radiative heat flux values are lower than the measured value by a factor of at least four.

Nomenclature

B_λ	=	blackbody (Planck) function at given wavelength λ, W/(cm^2-sr-μm)
D_n	=	exponential integral function of order n
E_n	=	exponential integral function of order n
I_λ	=	radiation intensity at given wavelength λ, W/(cm^2-sr-μm)
i	=	direction of propagation of radiation; see Figs. 1 and 2
ℓ	=	directional cosine
q, $q_{\rm rad}$	=	radiative heat flux, W/cm^2
s	=	coordinate for radiative transfer
T	=	temperature, K
θ	=	angle; see Figs. 1–3
κ_λ	=	absorption coefficient at given wavelength including stimulated emission, cm^{-1}
τ	=	optical depth measured from a reference point
ϕ	=	angle; see Figs. 1–3
ψ	=	angle; see Figs. 2 and 3

Subscripts

G	=	gray-gas mean
P	=	Planck mean
R	=	Rosseland mean
w	=	wall
λ	=	wavelength, μm

Introduction: Status of Radiation-Coupled Flowfield Solutions

A NUMBER of planetary missions are presently being planned, and some will be launched in the near future. Some of these include an Earth-return mission. Well-known examples are the Stardust mission[1] being carried out by the United States, the MUSES-C mission[2] planned by Japan, and the Rosetta mission[3] considered in Europe. When the space vehicles enter into the Earth's atmosphere on return from such missions, the absolute velocity of the vehicle becomes typically 12.5 km/s. The heating rate to the vehicle along the reentry trajectory becomes very large. Developing a reliable thermal protection system for such an entry is a prerequisite to the success of the missions. The design of such a thermal protection system requires accurate prediction of the heating environments.

A significant portion of the heat flux incident on the heatshield wall for such a vehicle will be by radiation because the temperature in the shock layer over the vehicle becomes very high, and the gas within the shock layer strongly radiates. In such a strongly radiating flowfield, radiation affects the flowfield properties, which in turn affect radiative properties. This coupling effect may be significant at high-speed entries. For such a case, the flowfield must be calculated accounting for the radiation–flow coupling phenomenon.

There are at least three reasons why calculation of the flowfield strongly affected by radiation is difficult:

1) There is spectral complexity. The absorption coefficients of the gas strongly depends on wavelength. Accurate line-by-line calculation of radiation requires wavelength points of the order of 1×10^6. Evaluating the absorption coefficients and calculating the transport of radiative energy at all of these wavelength regions is very time consuming. Earlier, several multiband models, which utilize only a few thousand wavelength points, have been introduced to reduce the computing time for the line-by-line method. Attempts have been made to solve the radiation-dominated flowfields using such a model.[4–7] Such works have shown that the computing time becomes very large with a multiband model, even for one-dimensional calculation, when radiation is fully coupled.[4,5]

2) There is a long-range effect. Radiative transport occurs over large distances, and the expression of the radiative source becomes a spatial integration of radiative properties. As a result, the governing equations become a set of nonlinear integro–differential equations. In conventional computational fluid dynamics, there are no established ways of ensuring convergence in the presence of such a long-range effect. In solving the flowfields other than a one-dimensional flow, only the so-called weakly coupled method has been tried to date.[6–8] In a weakly coupled method, the long-range effect is accounted for through an iteration procedure. The method has been shown to converge to a steady solution in a modestly strong radiating flowfield. However, no stability analysis has yet been made of the method to show its stability and convergence. In a strongly radiating flowfield, convergence of the weakly coupled method is not guaranteed.

3) There is multidimensionality. In the past, for such radiation-coupled calculations, the radiative transport equation was solved using the so-called tangent slab approximation, that is, radiative transport was assumed to occur only in the normal direction in an

Presented as Paper 99-0222 at the 37th Aerospace Sciences Meeting, Reno, NV, 11–14 January 1999; received 29 March 2000; revision received 28 August 2000; accepted for publication 29 August 2000.

*Graduate Student, Department of Aeronautics and Space Engineering; currently NRC Research Associate, Mail Stop 230-2, Reacting Flow Environments Branch, NASA Ames Research Center, Moffett Field, CA 94035. Student Member AIAA.

†Graduate Student, Department of Aeronautics and Space Engineering.

‡Professor, Department of Aeronautics and Space Engineering. Senior Member AIAA.

infinite slab layer tangent to the wall.[4–7] When radiation is very strong, radiative transfer from the stagnation region of a vehicle to the frustum region could raise temperature in the downstream region. To account for such phenomena, a more rigorous radiation calculation accounting for multidimensional radiative transfer is required.

Attempts have been made in the past to calculate a multidimensional radiating flowfield.[8,9] Hartung and Hassan employed an approximate radiation calculation method that reduced the governing equations from the integro–differential equations to partial differential equations.[8] In general, such a conversion is possible only if the optical thickness of the gas satisfies certain limiting conditions, and it is not valid generally for realistic entry conditions. Even with such a simplification, coupling was not accounted for in Ref. 8. Elbert and Cinnela developed a two-dimensional algorithm for radiation calculation.[9] However, they were able to implement the algorithm only for a gray-gas case. To the best of the authors' knowledge, two-dimensional fully coupled calculation accounting for a nongray nature of the gas in the shock layer has not yet been carried out.

Planck–Rosseland–Gray (PRG) Model and Strong Coupling

To overcome the problem arising from the spectral complexity, the Planck–Rosseland–gray (PRG) model has been developed.[10,11] At certain wavelengths, the radiation phenomenon is nearly optically thin. For such a wavelength, the Planck approximation is valid. For wavelengths for which radiation is optically thick, the Rosseland approximation is valid. In between these limits, gray-gas approximation becomes valid. In the PRG model, the Planck, the Rosseland, and the gray-gas approximations are combined.[10] This model can closely reproduce the radiative heat flux values obtained by a detailed line-by-line calculation.[10] The model has reduced the computing time of the multiband model at least by a factor of 10.

The PRG model has been used in solving a one-dimensional flowfield in Ref. 11. By expressing the radiative source as a spatial integration of radiative properties, and by discretizing, an implicit time-marching system of conservation equations is derived in the form of a fully loaded system of linear algebraic equations. The increment vector is obtained by inverting this equations set. When this is done, the long-range effect of radiation is fully implicitly accounted for.

The method was used in calculating a one-dimensional time-dependent radiating flowfield in the reflected shock region of a shock tube.[11] The method has been successfully applied for a very strongly radiating flowfield. The calculated results were compared with existing experimental data.[11] The calculation overestimated the measured values by a factor of slightly under two. The discrepancy was attributed to the radiation absorption occurring in the instrument. When this absorption is accounted for, good agreement was obtained between the calculation and the experiment.

The objective of the present work is to extend the one-dimensional method developed earlier and to develop a stable, converging method for calculating a strongly radiating axisymmetric flowfield over a blunt body. The PRG model is used in evaluating the spectral parameters of the problem as before, and a fully coupled, fully time-implicit solution scheme is developed for the axisymmetric flowfield. Radiative transfer is treated one, two, or three dimensionally. Thermochemical equilibrium (with 11 species for air and 17 species for the carbon-laden case) is assumed, and the viscous phenomenon is neglected in the present work because nonequilibrium and viscous phenomenon are not essential to the convergence issue at hand. Besides, strong radiation occurs usually at high densities where flow tends to approach equilibrium.

First, convergence and robustness of the developed method is confirmed for high-speed flow (13.4 and 16 km/s) conditions, for which no converged solution has been obtained to date. Then, comparison is made among the one-dimensional, two-dimensional, and three-dimensional radiative transport models, which leads to a certain conclusion. The effect of mesh size is tested also, to conclude that, for the inviscid stagnation-point flow under consideration, 15×15 mesh is adequate.

The computation method developed intermittently carries out a radiative transport calculation using a multiband model to determine the needed PRG parameters. As a result, the radiative heat flux calculated by the PRG model is always the same as that calculated by the multiband model. Therefore, the radiative calculation made in the PRG method is always accurate to the accuracy of the multiband model.

An experimental verification of the accuracy of the present method is sought by comparing the calculation with only existing experimental data obtained in a strongly radiating regime (13.4 km/s) (Ref. 12). In the experiment, radiation emanating from the shock layer over a flying model was measured in a combined ballistic range–shock tunnel facility. The models were spherically nosed cylinders with 0.5 cm radius and 0.7 cm cylinder diameter and were made of either polyethylene, polycarbonate, or aluminum. At lower flight speeds, spectra of the radiation emanating from the shock layer have been obtained.[13]

Surprisingly, the calculated radiation intensity is found to be under one-quarter of the measured value. One could possibly question the nonequilibrium effect. However, it is known that the nonequilibrium effect lowers radiation emission in such a speed range.[14] Therefore, if a nonequilibrium phenomenon existed in the experimental environment, the present equilibrium model should overestimate radiation intensity. The trend is also the opposite of that observed for the reflected-shock case[11] mentioned earlier.

An effort is expended, therefore, to find the possible causes of this discrepancy. Following an earlier hypothesis that models ablate during the flight in a ballistic range[13] and that ablation products radiate, the calculation is repeated with carbon added to air. Even then, the calculated radiation is only about one-quarter of the measured value. In addition, the scatter in the experimental data was relatively large (a factor of 6 between the highest and the lowest values). Thus, experimental confirmation of the accuracy of the present method is rendered unachieved and is left as a future task.

Formulation

One-Dimensional Radiative Transfer

Let us consider the coordinate system shown schematically in Fig. 1. In the one-dimensional case, the value of I_λ at a given point s and a given direction ϕ is independent of θ. Therefore, we can write

$$I_\lambda = I_\lambda(s, \phi) \tag{1}$$

The radiative transfer equation becomes

$$\cos\phi \frac{\partial I_\lambda}{\partial s} = \kappa_\lambda (B_\lambda - I_\lambda) \tag{2}$$

Radiative heat flux is given by

$$q_\lambda = \int I_\lambda \cos\phi \, \mathrm{d}\Omega \tag{3}$$

Because $\mathrm{d}\Omega = \sin\phi \, \mathrm{d}\theta \, \mathrm{d}\phi$, one obtains

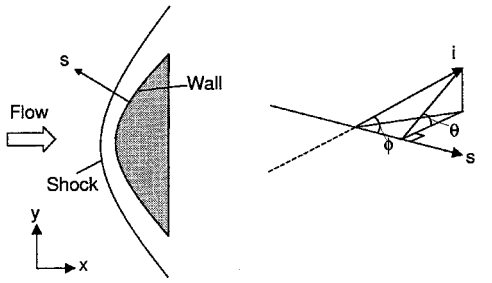

Fig. 1 Coordinate system for one-dimensional radiative transfer.

$$
\begin{aligned}
q_\lambda &= \int I_\lambda \cos\phi \, \mathrm{d}\Omega \\
&= \int_0^{2\pi} \int_0^{\pi} I_\lambda \cos\phi \sin\phi \, \mathrm{d}\phi \, \mathrm{d}\theta \\
&= 2\pi \int_0^{\pi} I_\lambda \cos\phi \sin\phi \, \mathrm{d}\phi \\
&= 2\pi \int_0^{\pi/2} I_\lambda^+ \cos\phi \, \mathrm{d}(-\cos\phi) + 2\pi \int_{\pi/2}^{\pi} I_\lambda^- \cos\phi \, \mathrm{d}(-\cos\phi) \\
&= 2\pi \int_0^1 I_\lambda^+ \ell \, \mathrm{d}\ell - 2\pi \int_0^{-1} I_\lambda^- \ell \, \mathrm{d}\ell \\
&= q_\lambda^+ + q_\lambda^-
\end{aligned}
$$

where

$$
q_\lambda^\pm = \pm 2\pi \int_0^{\pm 1} I_\lambda^\pm \ell \, \mathrm{d}\ell
$$

and $\ell = \cos\phi$. The sign + denotes the direction from the wall to the shock wave and the sign − denotes the direction from the shock wave to the wall. Total radiative heat flux is obtained as

$$
\begin{aligned}
q &= \int q_\lambda \, \mathrm{d}\lambda \\
&= q^+ + q^- \qquad (4)
\end{aligned}
$$

where

$$
q^\pm = \pm 2\pi \int_0^{\pm 1} I^\pm \ell \, \mathrm{d}\ell
$$

$$
I^\pm = \int I_\lambda^\pm \, \mathrm{d}\lambda
$$

In the PRG model, an absorption coefficient at a given wavelength point at a given cell in a flowfield is classified into one of the PRG means. The classification is achieved by using selection criteria.[10,11] Three mean absorption coefficients are then obtained in each group. The radiative heat fluxes are computed in each group, and the true value of radiative heat flux is given by a sum of each radiative heat flux for three groups. The radiative heat flux is given by

$$
q_{\mathrm{rad}}^{\mathrm{1D}} = q_{\mathrm{PRG}}^+ + q_{\mathrm{PRG}}^- \qquad (5)
$$

where

$$
\begin{aligned}
q_{\mathrm{PRG}}^\pm &= \pm 2\pi \int_0^{\pm} \left(I_P^\pm + I_R^\pm + I_G^\pm \right) \ell \, \mathrm{d}\ell \\
&= q_P^\pm + q_R^\pm + q_G^\pm
\end{aligned}
$$

The three components of the radiative heat flux in this expression, that is, those corresponding to Planck (P), Rosseland (R), and gray-gas (G) approximations are

$$
q_P^\pm = \pm \pi I_{P_b} + 2\pi \int_{s_b}^{s} \kappa_P B_P \, \mathrm{d}\hat{s} \qquad (6)
$$

$$
q_R^\pm = \pm \pi B_R - \frac{2}{3}\pi \left[\left(\frac{\mathrm{d}B}{\mathrm{d}T} \right)_R \Big/ \kappa_R \right] \frac{\mathrm{d}T}{\mathrm{d}s} \qquad (7)
$$

$$
q_G^\pm = \pm 2\pi I_{G_b} E_3(|\tau - \tau_b|) + 2\pi \int_{s_b}^{s} \kappa_G B_G E_2(|\tau - \hat{\tau}|) \, \mathrm{d}\hat{s} \qquad (8)
$$

where

$$
\tau(s) = \int_{s_w}^{s} \kappa_G \, \mathrm{d}\hat{s}
$$

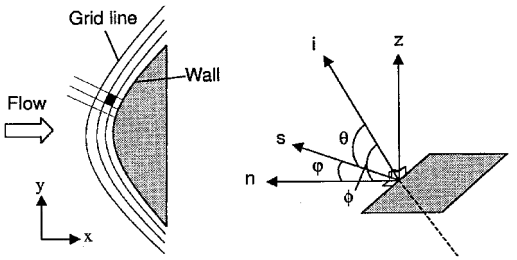

Fig. 2 Coordinate system for two-dimensional radiative transfer.

in which the subscripts b and w are the values of a boundary (wall or freestream) and wall, respectively, and E_n are the exponential functions,

$$
E_n(z) = \int_0^1 \ell^{n-2} \exp\left(-\frac{z}{\ell} \right) \mathrm{d}\ell
$$

$$
E_n'(z) = -E_{n-1}(z), \qquad n > 1
$$

The exponential functions are given by a truncated series expansion given in Ref. 15.

Two-Dimensional Radiative Transfer

The coordinate system is shown schematically in Fig. 2. In the two-dimensional case, radiative transfer is solved along each direction φ that is involved in the two-dimensional computational plane. Therefore, we can write

$$
I_\lambda = I_\lambda(s, \theta)_\varphi \qquad (9)
$$

The radiative transport equation becomes

$$
\cos\theta \frac{\partial I_\lambda}{\partial s} = \kappa_\lambda (B_\lambda - I_\lambda) \qquad (10)
$$

The formal solution is obtained as

$$
I_\lambda(s) = I_\lambda(s_{\mathrm{in}}) \exp\left(-\frac{\tau_\lambda - \tau_{\lambda_{\mathrm{in}}}}{\cos\theta} \right) + \int_{s_{\mathrm{in}}}^{s} \frac{\kappa_\lambda B_\lambda}{\cos\theta} \exp\left(-\frac{\tau_\lambda - \hat{\tau}_\lambda}{\cos\theta} \right) \mathrm{d}\hat{s} \qquad (11)
$$

where

$$
\tau_\lambda = \int_{s_{\mathrm{in}}}^{s} \kappa_\lambda \, \mathrm{d}s
$$

and the subscript in denotes an inner boundary. From Fig. 2, we have

$$
\cos\phi = \cos\theta \cos\varphi
$$

$$
\mathrm{d}\Omega = \cos\theta \, \mathrm{d}\varphi \, \mathrm{d}\theta
$$

Radiative heat flux is then calculated by

$$
\begin{aligned}
q_\lambda &= \int I_\lambda \cos\phi \, \mathrm{d}\Omega \\
&= \int_{-\pi/2}^{3\pi/2} \cos\varphi \int_{-\pi/2}^{\pi/2} I_\lambda \cos^2\theta \, \mathrm{d}\theta \, \mathrm{d}\varphi \\
&= \int_{-\pi/2}^{\pi/2} \cos\varphi \int_{-\pi/2}^{\pi/2} I_\lambda^+ \cos^2\theta \, \mathrm{d}\theta \, \mathrm{d}\varphi \\
&\quad + \int_{\pi/2}^{3\pi/2} \cos\varphi \int_{-\pi/2}^{\pi/2} I_\lambda^- \cos^2\theta \, \mathrm{d}\theta \, \mathrm{d}\varphi \\
&= \int_{-\pi/2}^{\pi/2} \cos\varphi \int_{-\pi/2}^{\pi/2} I_\lambda^+ \cos^2\theta \, \mathrm{d}\theta \, \mathrm{d}\varphi \\
&\quad - \int_{-\pi/2}^{\pi/2} \cos\varphi \int_{-\pi/2}^{\pi/2} I_\lambda^- \cos^2\theta \, \mathrm{d}\theta \, \mathrm{d}\varphi \\
&= q_\lambda^+ + q_\lambda^-
\end{aligned}
$$

where

$$q_\lambda^{\pm} = \pm \int_{-\pi/2}^{\pi/2} \cos\varphi \int_{-\pi/2}^{\pi/2} I_\lambda^{\pm} \cos^2\theta \, \mathrm{d}\theta \, \mathrm{d}\varphi$$

The sign + denotes the direction from an inner boundary to a given point, and the sign − is the opposite direction. The total radiative heat flux is given by

$$q = \int q_\lambda \, \mathrm{d}\lambda = q^+ + q^- \tag{12}$$

where

$$q^{\pm} = \pm \int_{-\pi/2}^{\pi/2} \cos\varphi \int_{-\pi/2}^{\pi/2} I^{\pm} \cos^2\theta \, \mathrm{d}\theta \, \mathrm{d}\varphi \tag{13}$$

The radiative heat fluxes for each directions in the PRG model are given, respectively, as

$$q_{\mathrm{PRG}}^{\pm} = \pm \int_{-\pi/2}^{\pi/2} \cos\varphi \int_{-\pi/2}^{\pi/2} \left(I_P^{\pm} + I_R^{\pm} + I_G^{\pm}\right) \cos^2\theta \, \mathrm{d}\theta \, \mathrm{d}\varphi$$

$$= q_P^{\pm} + q_R^{\pm} + q_G^{\pm}$$

and

$$q_{\mathrm{rad}}^{\mathrm{2D}} = q_{\mathrm{PRG}}^{+} + q_{\mathrm{PRG}}^{-} \tag{14}$$

The components of the heat fluxes are

$$q_P^{\pm} = \pm 2 \int_{-\pi/2}^{\pi/2} \cos\varphi \left\{ \frac{\pi}{4} I_{P_b} \pm \int_{s_b}^{s} \kappa_P B_P \, \mathrm{d}\hat{s} \right\} \mathrm{d}\varphi \tag{15}$$

$$q_R^{\pm} = \pm \pi B_R - \frac{4}{3} \frac{1}{\kappa_R} \left(\frac{\mathrm{d}B}{\mathrm{d}T} \right)_R \int_{-\pi/2}^{\pi/2} \frac{\mathrm{d}T}{\mathrm{d}s} \cos\varphi \, \mathrm{d}\varphi \tag{16}$$

$$q_G^{+} = \pm 2 \int_{-\pi/2}^{\pi/2} \cos\varphi \left\{ I_{G_b} D_2(|\tau - \tau_b|) \right.$$

$$\left. \pm \int_{s_b}^{s} \kappa_G B_G D_1(|\tau - \hat{\tau}|) \, \mathrm{d}\hat{s} \right\} \mathrm{d}\varphi \tag{17}$$

where

$$\tau(s) = \int_{s_{\mathrm{in}}}^{s} \kappa_G \, \mathrm{d}\hat{s}$$

and

$$D_n(z) = \int_0^{\pi/2} \exp\left(-\frac{z}{\cos\theta} \right) \cos^n\theta \, \mathrm{d}\theta \tag{18}$$

This exponential integral is evaluated by numerical integration.

Three-Dimensional Radiative Transfer

In the three-dimensional case (Fig. 3), we can write

$$I_\lambda = I_\lambda(s, \theta, \varphi) \tag{19}$$

The equation of radiative transfer becomes

$$\frac{\partial I_\lambda}{\partial s} = \kappa_\lambda (B_\lambda - I_\lambda) \tag{20}$$

The formal solution is given by

$$I_\lambda(s) = I_\lambda(s_{\mathrm{in}}) \exp\left[-\left(\tau_\lambda - \tau_{\lambda_{\mathrm{in}}}\right) \right] + \int_{s_{\mathrm{in}}}^{s} \kappa_\lambda B_\lambda \exp[-(\tau_\lambda - \hat{\tau}_\lambda)] \, \mathrm{d}\hat{s} \tag{21}$$

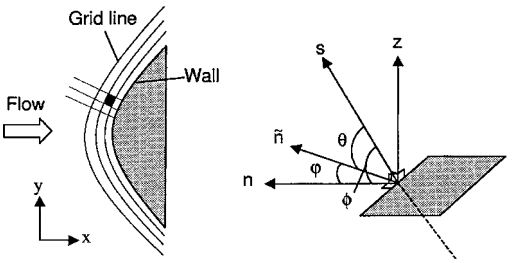

Fig. 3 Coordinate system for three-dimensional radiative transfer.

where

$$\tau_\lambda = \int_{s_{\mathrm{in}}}^{s} \kappa_\lambda \, \mathrm{d}s \tag{22}$$

The total radiative heat flux is given by Eqs. (13). The components of the radiative heat fluxes are

$$q_P^{\pm} = \pm \int_{-\pi/2}^{\pi/2} \cos\varphi \int_{-\pi/2}^{\pi/2} \left\{ I_{P_b} \pm \int_{s_b}^{s} \kappa_P B_P \, \mathrm{d}\hat{s} \right\} \cos^2\theta \, \mathrm{d}\theta \, \mathrm{d}\varphi \tag{23}$$

$$q_R^{\pm} = \pm \pi B_R - \frac{1}{\kappa_R} \left(\frac{\mathrm{d}B}{\mathrm{d}T} \right)_R \int_{-\pi/2}^{\pi/2} \cos\varphi \int_{-\pi/2}^{\pi/2} \frac{\mathrm{d}T}{\mathrm{d}s} \cos^2\theta \, \mathrm{d}\theta \, \mathrm{d}\varphi \tag{24}$$

$$q_G^{\pm} = \pm \int_{-\pi/2}^{\pi/2} \cos\varphi \int_{-\pi/2}^{\pi/2} \left\{ I_{G_b} \exp(-|\tau - \tau_b|) \right.$$

$$\left. \pm \int_{s_b}^{s} \kappa_G B_G \exp(-|\tau - \hat{\tau}|) \, \mathrm{d}\hat{s} \right\} \cos^2\theta \, \mathrm{d}\theta \, \mathrm{d}\varphi. \tag{25}$$

The total radiative heat flux is

$$q_{\mathrm{rad}}^{\mathrm{3D}} = q_{\mathrm{PRG}}^{+} + q_{\mathrm{PRG}}^{-} \tag{26}$$

Multiband Model

A multiband model is used in the PRG model to construct absorption coefficients, along with the tangent slab approximation and to determine the characteristic parameters needed in the PRG model.[10] In the multiband model, the absorption coefficients are evaluated at 2294 wavelength points for air for the wavelength region from 750 to 15,000 Å. For the carbon-containing species, the absorption coefficients are evaluated at 4060 wavelength points in the present work. The absorption coefficient of the gas mixture is expressed as a sum of those for individual species in the form[4]

$$\kappa_\lambda = \sum_i n_i \sigma_{\lambda i} \tag{27}$$

where n_i is the number density of species i and $\sigma_{\lambda i}$ is the absorption cross section. The cross-section value is curve fitted using the five parameters in the form

$$\sigma_{\lambda i} = \exp\left(A_{\lambda_1}^i \big/ z + A_{\lambda_2}^i + A_{\lambda_3}^i \ln z + A_{\lambda_3}^i z + A_{\lambda_5}^i z^2 \right) \tag{28}$$

where $z = 10{,}000/T$.

For air, the radiation from N, O, N_2, O_2, NO, and N_2^+ is accounted for. For the case where carbon is added, the radiation from C, CN, CO, and C_2 is additionally considered.

Numerical Method

The conservation equations governing the flowfield can be written as

$$\frac{\partial \boldsymbol{Q}}{\partial t} + \frac{\partial \boldsymbol{E}}{\partial x} + \frac{\partial \boldsymbol{F}}{\partial y} + \boldsymbol{G} = \boldsymbol{F}_{\mathrm{rad}} \tag{29}$$

where $\boldsymbol{Q}$ are the conservative variables, $\boldsymbol{E}$ and $\boldsymbol{F}$ are the convective flux vectors, $\boldsymbol{G}$ are the source vectors for axisymmetric flows, and $\boldsymbol{F}_{\text{rad}}$ are the source vectors for radiation.

A finite volume upwind method is employed for discretizing Eq. (29). The numerical flux function is evaluated by the Steger–Warming flux vector splitting method.[16] The flux Jacobian is split by the conventional flux vector splitting technique.[17] The detailed numerical formulation is given in Ref. 17 and, therefore, is omitted here. A direct matrix inversion is used to integrate Eq. (29) in time.

As is stated in the Introduction, the flowfield is assumed to be thermochemical equilibrium in the present study. The equilibrium gas properties are fed into the flow solver in a table.[18] The table values are determined by the free energy minimization method.

When radiative transfer is calculated by using the tangent slab approximation, that is, radiative transfer occurs only through the direction normal to the body, the source vector for radiation, $\boldsymbol{F}_{\text{rad}}$, is given by

$$\boldsymbol{F}_{\text{rad}} = \frac{\partial \boldsymbol{Q}_{\text{rad}}}{\partial \boldsymbol{s}} \tag{30}$$

where

$$\boldsymbol{Q}_{\text{rad}} = \begin{pmatrix} 0 \\ 0 \\ 0 \\ -q_{\text{rad}} \end{pmatrix} \tag{31}$$

and $\boldsymbol{s}$ is the unit normal vector to the body surface. Integrating the right-hand side of Eq. (29) in the jth computational cell, one obtains

$$\begin{aligned} \int_S \boldsymbol{F}_{\text{rad}}\, \mathrm{d}S &= \int_S \frac{\partial \boldsymbol{Q}_{\text{rad}}}{\partial \boldsymbol{s}}\, \mathrm{d}S \\ &= \sum \boldsymbol{Q}_{\text{rad}} (\boldsymbol{s}_x \cdot n_x + \boldsymbol{s}_y \cdot \boldsymbol{n}_y)\, \Delta \boldsymbol{s} \\ &= \sum \boldsymbol{Q}_{\text{rad}}^{\text{1D}} n_s\, \Delta \boldsymbol{s} \end{aligned} \tag{32}$$

where $\boldsymbol{Q}_{\text{rad}}^{\text{1D}}$ is the radiative heat flux at the cell interface of the jth computational cell. The integration is carried out in the normal direction $\boldsymbol{s}$ to the body surface within the slab layer tangent to the surface. The component of $\boldsymbol{Q}_{\text{rad}}^{\text{1D}}$ is given by Eq. (5) and $n_s = \pm 1$.

In a multidimensional space, the source vector for radiation, $\boldsymbol{F}_{\text{rad}}$, becomes

$$\boldsymbol{F}_{\text{rad}} = \frac{\partial \boldsymbol{Q}_{\text{rad}_x}}{\partial x} + \frac{\partial \boldsymbol{Q}_{\text{rad}_y}}{\partial y} + r \frac{\boldsymbol{Q}_{\text{rad}_y}}{y} \tag{33}$$

where

$$\boldsymbol{Q}_{\text{rad}_x} = \begin{pmatrix} 0 \\ 0 \\ 0 \\ -q_{\text{rad}_x} \end{pmatrix}, \qquad \boldsymbol{Q}_{\text{rad}_y} = \begin{pmatrix} 0 \\ 0 \\ 0 \\ -q_{\text{rad}_y} \end{pmatrix} \tag{34}$$

and $r = 1$ for three-dimensional case and $r = 0$ for two-dimensional case. Note that the flowfield is always assumed to be axisymmetric. Integration of the radiative source over the cell volume becomes, for example, in three dimensions

$$\begin{aligned} \int_S \boldsymbol{F}_{\text{rad}}\, \mathrm{d}S &= \int_S \left(\frac{\partial \boldsymbol{Q}_{\text{rad}_x}}{\partial x} + \frac{\partial \boldsymbol{Q}_{\text{rad}_y}}{\partial y} + \frac{\boldsymbol{Q}_{\text{rad}_y}}{y} \right) \mathrm{d}S \\ &= \int_{\partial S} \left(\boldsymbol{Q}_{\text{rad}_x} n_x + \boldsymbol{Q}_{\text{rad}_y} n_y \right) \mathrm{d}\boldsymbol{s} + \int_S \frac{\boldsymbol{Q}_{\text{rad}_y}}{y}\, \mathrm{d}S \\ &= \sum (\boldsymbol{Q}_{\text{rad}_x} n_x + \boldsymbol{Q}_{\text{rad}_y} n_y) \Delta \boldsymbol{s} + \frac{\hat{\boldsymbol{Q}}_{\text{rad}_y}}{y} \Delta \boldsymbol{S} \\ &= \sum \hat{\boldsymbol{Q}}_{\text{rad}}^{\text{3D}} \Delta \boldsymbol{s} + \frac{\hat{\boldsymbol{Q}}_{\text{rad}_y}}{y} \Delta S \end{aligned} \tag{35}$$

where

$$\hat{\boldsymbol{Q}}_{\text{rad}}^{\text{3D}} = \boldsymbol{Q}_{\text{rad}_x} n_x + \boldsymbol{Q}_{\text{rad}_y} n_y \tag{36}$$

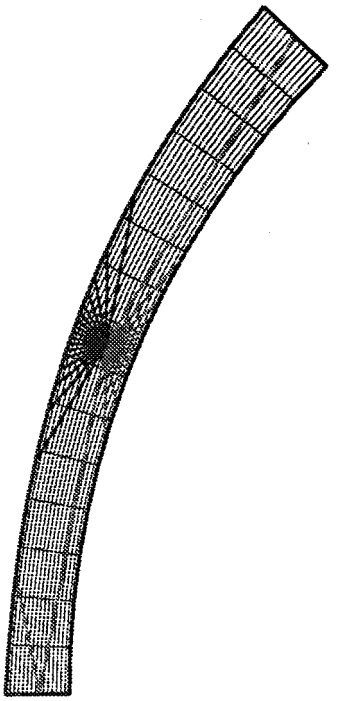

Fig. 4 Typical example of two-dimensional radiation rays and computational mesh (15 × 15).

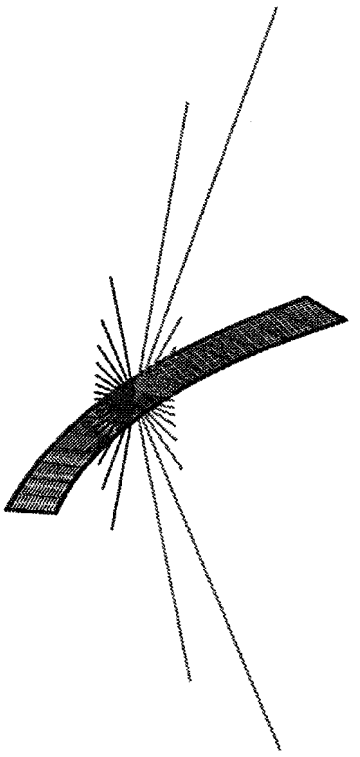

Fig. 5 Typical example of three-dimensional radiation rays (only the rays in the selected plane perpendicular to computational plane are shown).

$$\hat{\boldsymbol{Q}}_{\text{rad}_y} = \frac{\int_S \boldsymbol{Q}_{\text{rad}_y}\, \mathrm{d}S}{\int_S \mathrm{d}S} \tag{37}$$

$\hat{\boldsymbol{Q}}_{\text{rad}}^{\text{3D}}$ at each cell interface is calculated by solving the radiative transfer equations and integrating over the solid angle defined by those rays.

In Figs. 4 and 5, which show computational grid used, rays for two-dimensional and three-dimensional cases, respectively, are shown schematically. In the two-dimensional case, the rays emanate from each cell interface to a boundary at 10-deg intervals from −170 to 170 deg on the computational domain. Because the flow properties should be the same across a symmetry plane, the radiation rays are reflected at the symmetry plane for the two-dimensional case. For

each direction, 17 radiation rays are used. In the three-dimensional case, the rays are emanated from each cell interface at 10-deg intervals in all global directions. The number of 289 radiation rays is employed for this case.

The coupling calculation for the multidimensional case is performed as follows: A converged solution is obtained for an inviscid flow without radiation. The PRG model is then constructed for this flowfield. To do this, the radiative transport equation is first solved along each j line at constant i line, where i and j are spatial indices along the body and normal to the body, respectively. The values of the parameters in the PRG model, that is, the criteria used in determining the three optical regimes in the model, are determined at each cell, assuming a tangent slab layer along the constant j line. The fully coupled calculation, in which radiation is treated in two or three dimensions, is then carried out using the PRG parameters so determined. If the temperature at a cell along the j line at a given constant i line is changed significantly, the PRG model is updated, and new selection criteria are obtained and applied along that j line.

Flow Conditions

To verify the accuracy of the present computation method by comparison with experimental data, the calculation is made for an existing set of experimental data. In the experiment, described in Refs. 12 and 13, 13.4-km/s flight velocity was attained by the counterflow technique using a combination of a ballistic range and a shock tunnel facility. The models were spherically nosed cylinders with 0.5 cm radius and 0.7 cm cylinder diameter and were made of either polyethylene, polycarbonate, or aluminum. In the present study, the shock-layer flows over this model at the freestream density of 5.5×10^{-4} kg/m^3 and the freestream velocity of 13.4 km/s. The same freestream density and the hypothetical velocity of 16 km/s are computed. A typical example of the computational grid is shown in Fig. 4. The boundary condition for the flow calculation are as follows: A slip condition is imposed at the wall. A zeroth-order extrapolation is used at the outflow boundary. A symmetry condition is given in the symmetry plane. The freestream condition is fixed at the inflow boundary.

The boundary condition for the radiation calculation is as follows: The farfield is also assumed to be a blackbody of freestream temperature of 300 K. The radiation from the downstream of the outflow boundary into the upstream direction is assumed to be zero. The wall is assumed to be a blackbody of 3000 K. This wall temperature is assumed to be a surface temperature for an ablating surface. The boundary value is included in the Planck part of the PRG model in the present study. Because the shock-layer temperature is the order of 10,000 K, the amount of wall blackbody radiation at this temperature is smaller than that of the radiation in the flowfield. Therefore, the overall effect of this wall blackbody radiation will be small in the present inviscid case.

Results and Discussion

General Features of the Solutions

Figure 6 shows the temperature contours for the one-dimensional radiation calculation. The temperature contours for the two- and three-dimensional calculations are nearly identical to those of the one-dimensional calculation and, therefore, are not shown here. Figure 7 shows the contours of the Planck mean absorption coefficients for the two-dimensional radiation calculation. The contours vary smoothly, implying the well-behaved nature of the present procedure. This suggests the validity of the present procedure of determining the PRG parameters for multidimensional radiation calculation from the one-dimensional (tangent slab) radiation field.

In Fig. 8, the convergence histories for one-, two-, and three-dimensional radiation calculations for the 16-km/s flight velocity case are compared. The results of different two sets of computational grids are shown in Fig. 8. For all cases, the residual decreases by at least two orders of magnitude within 4000 iterations. For a finer grid, convergences slow down, as expected.

In Fig. 9, the convergence histories of the radiative heat flux at the stagnation point toward the wall for one-, two-, and three-dimensional radiation calculations for the 16-km/s flight velocity

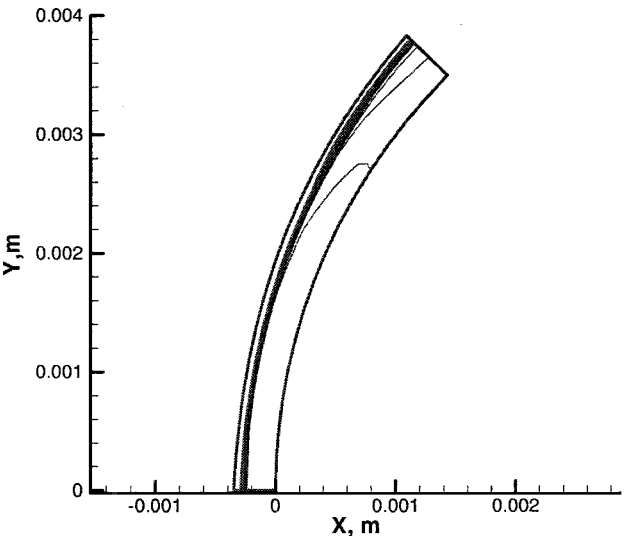

Fig. 6 Temperature contours for the 13.4-km/s flight velocity case.

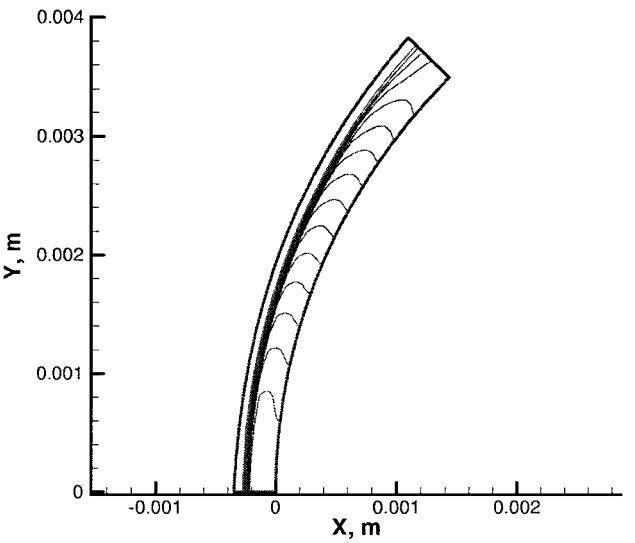

Fig. 7 Contours of Planck mean absorption coefficients for the 13.4-km/s flight velocity case.

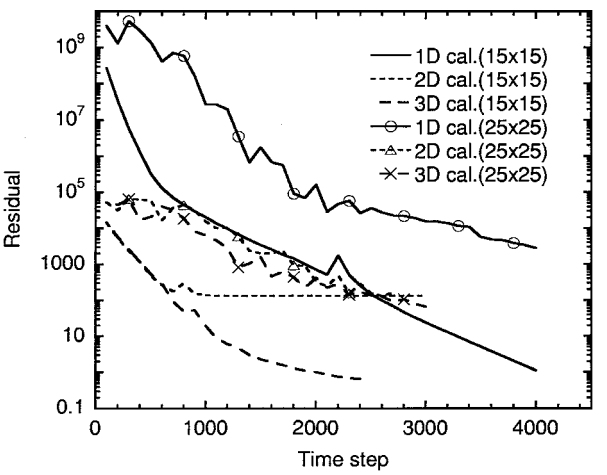

Fig. 8 Convergence histories for each radiative transfer model for one-, two-, and three-dimensional radiation calculations for the 16-km/s flight velocity case.

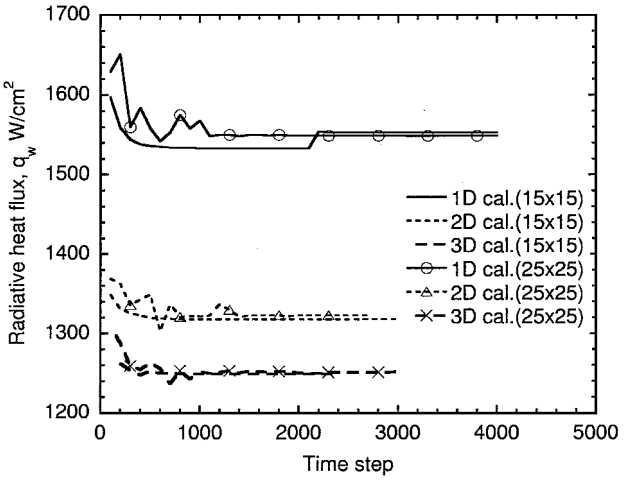

Fig. 9 Convergence histories of radiative heat flux at the stagnation point for one-, two-, and three-dimensional radiation calculations for the 16-km/s flight velocity case.

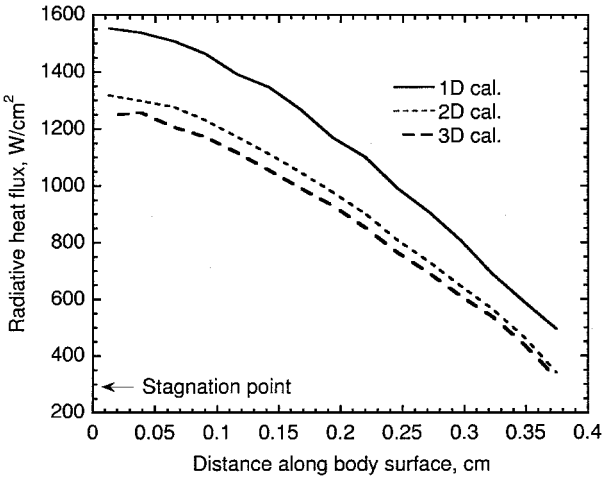

Fig. 11 Radiative heat flux distributions along the body surface for one-, two-, and three-dimensional radiation calculations for the 16-km/s flight velocity case.

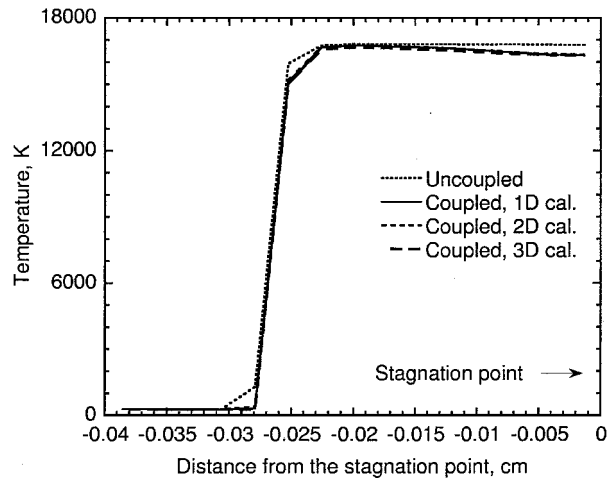

Fig. 10 Temperature distribution along the stagnation streamline for one-, two-, and three-dimensional radiation calculations and radiation uncoupled calculation for the 16-km/s flight velocity case.

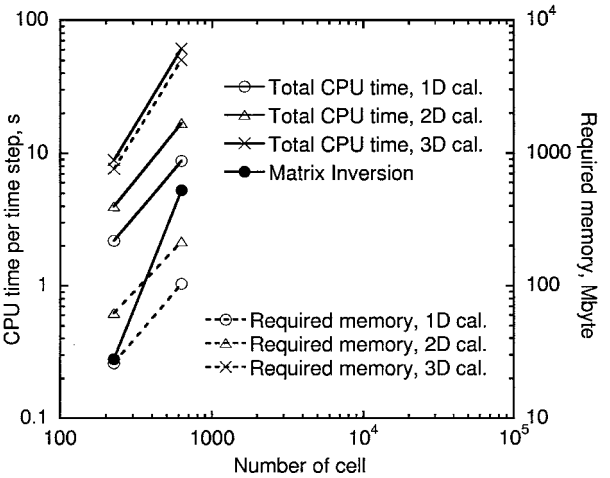

Fig. 12 Comparison of typical required CPU time and required memory for one-, two-, and three-dimensional radiation calculations.

case are shown. The histories are shown for both a coarse mesh (15×15 cells) and a finer mesh (25×25) in Fig. 9. The asymptotic values are obtained within 2000 iterations for both computational grids. The difference between the radiative heat flux values calculated with 15×15 cells and those with 25×25 cells are indistinguishably small. Therefore, the results with 15×15 cells are used for comparison with the experiment later.

Figure 10 shows the comparison of the temperature distribution along the stagnation streamline for one-, two-, and three-dimensional radiation calculations and the uncoupled calculation for the 16-km/s flight velocity case. There is no discernible difference in shock standoff distance between the coupled and uncoupled calculations, although the temperature behind the shock wave decreases toward the wall because of the radiative cooling effect.

Figure 11 shows comparison of the wall radiative heat flux along the body surface for one-, two-, and three-dimensional radiation calculations for the 16-km/s flight velocity case. The two- and three-dimensional calculations give consistently lower values than the tangent slab result. One can surmise that, in the multidimensional radiation calculation, radiative transfer occurs in the tangential direction, and some radiative power is lost through the exit boundary. This is particularly the case at the downstream region, where the radiative intensity from the outflow boundary is assumed to be zero.

The present codes are fully vectorized. In Fig. 12, the CPU time required per time step and required computational memory size against the number of cells are compared for one-, two- and three-dimensional radiation calculations. The CPU time expended in matrix inversion calculation, which is independent of the dimensions of radiation calculation, is also shown in Fig. 12. The results are presented for the cases with 15×15 and 25×25 cells. If the required memory can be linearly extrapolated with the grid size on this plot, the present one- or two-dimensional radiation calculation will require 1-GB memory size with a typical grid size of 100×50. However, the required memory for the three-dimensional radiation calculation will become prohibitively large for the same grid. One sees also that the required CPU time for matrix inversion increases rapidly and will be dominating for larger grid sizes. Because the results of the two-dimensional radiation calculation is not much different from that of the three-dimensional calculation, one concludes at this time that the best compromise would be to restrict the grid to about 100×50 and to use a two-dimensional calculation method.

Radiative Heat Flux at the Stagnation Point

The experimental data obtained in Ref. 12 show a scatter factor of 6. The logarithmic mean of the measured values is taken as the valid mean value. Table 1 shows comparison of the radiative heat flux at the stagnation point for air between the experiment for a polyethylene model and calculations obtained by one-, two-, and three-dimensional radiation-coupled codes, respectively.

The radiative heat flux is evaluated over the wavelength range from 2200 to 8500 Å. In all cases, calculated radiative heat flux values are lower than the measured value. The three-dimensional

Table 1 Comparison of radiative heat flux between experiments and calculations

Method	q_w, W/cm^2
Experiment	49.6
One-dimensional calculation (air)	10.9
Two-dimensional calculation (air)	9.8
Three-dimensional calculation cal (air)	9.0
One-dimensional calculation (0.2% of carbon mass)	12.8
One-dimensional calculation (2% of carbon mass)	12.7
One-dimensional calculation (20% of carbon mass)	11.8
Two-dimensional calculation (20% of carbon mass)	10.6
Three-dimensional calculation (20% of carbon mass)	9.4

calculation gives a value that is lower than the measured value by a factor of about five.

To explore the cause of the strong observed radiation, attention is paid first to an experimental result reported in Ref. 19. In Ref. 19, a spectroscopic observation was carried out for airflow over a flat disk model made of carbon-phenolic placed in an arc-jet wind tunnel. The test model was ablating. The spectroscopic observation was made of the region approximately 2 cm away from the model wall, which was within the inviscid region. The spectral radiation of the wavelength range from 3800 to 6200 Å was measured. The results showed that CN was the strongest radiator. CN is believed to be produced by the interaction between the carbon particles ejected from the wall during the ablation process and nitrogen in air. In Ref. 19, a calculation is carried out to show that carbon particles of typical sizes could indeed migrate far into the inviscid region and vaporize there to produce the observed CN radiation.

To test whether such a phenomenon could have produced the strong observed radiation, elemental carbon is assumed to exist in the freestream to a concentration by mass of 0.2, 2, and 20%. This leads to formation of C, CN, CO, C_2, C^+, and CO^+, in addition to the standard 11 species for ionized air. Radiation of these species (see subsection "One-Dimensional Radiative Transfer") is then added to the PRG model. The results are presented in Table 1. Because the one-dimensional radiation calculation gives the highest radiative heat flux value, one-dimensional radiation-coupled calculations are performed only for the 0.2 and 2% cases. The results show that the calculations still underestimate the experimental radiative heat flux by a factor of about four.

Because of the discrepancy between the calculation and the measurement, and because of the rather large scatter in the experimental data, experimental verification of the accuracy of the present method is rendered unachieved. There are no other independent means of verifying the accuracy of the present method. The well-known Tauber–Sutton formula[20] is not applicable here because the calculated condition is outside the valid range of the formula. However, as mentioned earlier in the second section, the present PRG method is automatically set within the calculation process to give the same result as the multiband method. The multiband method is verified against a rigorous line-by-calculation.[4,7] The PRG method is also validated for a shock tube experiment in Ref. 11. These stand presently as the only assurance of the accuracy of the present method. The discrepancy between the calculation and the experiment is a subject of a study by the present authors in a separate paper.[21]

Concluding Remarks

A strongly radiating shock layer flow over a blunt body can be calculated by a new method that is based on 1) the PRG radiation model, 2) multidimensional radiative transfer, 3) fully time-implicit integration, and 4) full spatial coupling through inversion of a fully loaded system of algebraic equations. Convergence to a steady solution is obtained for 16-km/s flight speed. Two- and three-dimensional radiation calculations show results that are significantly different from that of a one-dimensional calculation. A two-dimensional radiation calculation, which is practical to a 100×50 grid, gives a result close to a three-dimensional calculation. A 15×15 mesh is satisfactory in calculating the stagnation-point flow. When the method is tested against experimental data obtained in a ballistic range, the calculation underestimated the measured value by a factor of four, even when a hypothetical radiation from carbon is added.

Acknowledgments

The present research has been supported by JSPS Research Fellowships for Young Scientists. The first author would like to thank Chul Park for his helpful suggestions.

References

[1]Olynick, D., Chen, Y.-K., and Tauber, M. E., "Forebody TPS Sizing with Radiation and Ablation for the Stardust Sample Return Capsule," AIAA Paper 97-2474, June 1997.

[2]Ahn, H. K., and Park, C., 'Preliminary Study of the MUSES-C Reentry," AIAA Paper 97-0278, Jan. 1997.

[3]Desnoyer, D., Buck, C., and Larrieu, J. M., "CNSR Rosetta SEPCORE-A Breakthrough for Earth Reentry Capsule," International Astronautical Federation, IAF Paper 91-298, Oct. 1991.

[4]Park, C., and Milos, F. S., "Computational Equations for Radiating and Ablating Shock Layers," AIAA Paper 90-0356, Jan. 1990.

[5]Gökçen, T., and Park, C., "The Coupling of Radiative Transfer to Quasi-One-Dimensional Flows with Thermochemical Nonequilibrium," AIAA Paper 91-0570, Jan. 1991.

[6]Olynick, D. R., Henline, W. D., Chamber, L. H., and Candler, G. V., "Comparisons of Coupled Radiative Navier–Stokes Flow Solutions with the Project Fire II Flight Data," AIAA Paper 94-1955, June 1994.

[7]Gökçen, T., "Computation of Nonequilibrium Radiating Shock Layers," AIAA Paper 93-0144, Jan. 1993.

[8]Hartung, L. C., and Hassan, H. A., "Radiation Transport Around Axisymmetric Blunt Body Vehicles Using a Modified Differential Approximation," *Journal of Thermophysics and Heat Transfer*, Vol. 7, No. 2, 1993, pp. 220–227.

[9]Elbert, G. J., and Cinnela, P., "Two-Dimensional Radiative Heat-Transfer Calculations for Nonequilibrium Flows," *Journal of Spacecraft and Rockets*, Vol. 32, No. 2, 1995, pp. 231–240.

[10]Sakai, T., Sawada, K., and Park, C., "Assessment of Planck–Rosseland–Gray Model for Radiating Shock Layer," AIAA Paper 97-2560, June 1997.

[11]Sakai, T., Sawada, K., and Park, C., "Calculation of Radiating Flowfield Behind a Reflected Shock Wave in Air," *Journal of Thermophysics and Heat Transfer*, Vol. 13, No. 1, 1999, pp. 42–49.

[12]Canning, T. N., and Page, W. A., "Measurements of Radiation From the Flow Fields of Bodies Flying at Speeds Up to 13.4 Kilometers per Second," *The High Temperature Aspects of Hypersonic Flow*, AGARDograph 68, edited by W. C. Nelson, Pergamon, Oxford, England, U.K.,1964, pp. 569–582.

[13]Page, W. A., and Arnold, J. O., "Shock Layer Radiation of Blunt Bodies at Entry Velocities," NASA TR R-193, April 1964.

[14]Park, C.,"Review of Chemical-Kinetic Problems of Future NASA Missions. I: Earth Entries," *Journal of Thermophysics and Heat Transfer*, Vol. 7, No. 3, 1993, pp. 385–398.

[15]Abramowitz, M., and Stegum, I. A., *Handbook of Mathematical Functions*, National Bureau of Standards, Applied Mathematics Series 55, Washington, DC, 1964, pp. 227–251.

[16]Steger, J. L., and Warming, R. F., "Flux Vector Splitting of the Inviscid Gasdynamic Equations with Application to Finite-Difference Methods," *Journal of Computational Physics*, Vol. 40, No. 2, 1981, pp. 263–293.

[17]Sakai, T., "The Computation of Strongly Radiating Hypersonic Flowfields," Ph.D. Thesis, Dept. of Aeronautics and Space Engineering, Tohoku Univ., Sendai, Japan, March 1999.

[18]Sawada, K., and Dendou, E., "Validation of Hypersonic Equilibrium Flow Calculations Using Ballistic-Range Data," AIAA Paper 97-0344, Jan. 1997.

[19]Park, C., "Interaction of Spalled Particles with Shock Layer Flow," *Journal of Thermophysics and Heat Transfer*, Vol. 13, No. 4, 1999, pp. 441–449.

[20]Tauber, M. E., and Sutton, K., "Stagnation Point Radiative Heating Relations for Earth and Mars Entries," *Journal of Spacecraft and Rockets*, Vol. 28, No. 1, 1991, pp. 40–42.

[21]Sakai, T., and Sawada, K., "Calculation of Nonequilibrium Radiation from a Blunt Body Shock Layer," *Journal of Thermophysics and Heat Transfer*, Vol. 15, No. 1, 2000, pp. 99–105.